Crystal structures and magnetic properties of iron borates containing lanthanides $Sr_6LnFe(BO_3)_6$ (*Ln* = La, Pr, Nd, Sm–Lu)

Hiroki Inoue, Yoshihiro Doi*, and Yukio Hinatsu

Division of Chemistry, Graduate School of Science, Hokkaido University, Sapporo 060-0810, Japan

*Corresponding Author: Yoshihiro Doi

Division of Chemistry,
Graduate School of Science,
Hokkaido University,
Sapporo 060-0810, Japan.
TEL: +81-11-706-2715
FAX: +81-11-706-4931
E-mail: doi@sci.hokudai.ac.jp

Abstract

The crystal structures and magnetic properties of borate compounds $Sr_6LnFe(BO_3)_6$ (*Ln* = La, Pr, Nd, Sm–Lu) were investigated. These compounds crystallize in a hexagonal structure with space group $R\bar{3}$, in which the *Ln* and Fe ions form one-dimensional chain structure. From the results of structural analysis, it was found that there is an anti-site disorder between Sr and *Ln* sites, and its chemical formula can be represented as $(Sr_{6-x}Ln_x)(Ln_{1-x}Sr_x)Fe(BO_3)_6$. The value of *x* increases with ionic radius of Ln^{3+}. The results of magnetic susceptibility measurements show that all the $Sr_6LnFe(BO_3)_6$ are paramagnetic, and the onset of an antiferromagnetic ordering was observed below ~3 K from the specific heat measurements.

Keywords: Borate, Lanthanide, One-dimensional chain structure, Magnetic properties, Magnetic susceptibility, Specific heat

Introduction

Recently, the borate crystals containing both lanthanide (*Ln*) and transition metal (*M*) ions attract great deal of interests because of their characteristic crystal structures and physical properties. For example, the family of $LnM_3(BO_3)_4$ borates have been extensively studied because they show interesting optical properties [1,2], structural and magnetic phase transitions [3], and multiferroic behavior [4]. In addition, the dolomite-type borates $LnM(BO_3)_2$ (*Ln* = Y, Ho–Lu; *M* = Cr) having an alternating connecting structure of LnO_6 and CrO_6 octahedra show an antiferromagnetic behavior at low temperatures [5].

Among such compounds, we focused our attention on a group of $A_6MM'(BO_3)_6$ borates [6–8]. They have a hexagonal unit cell (space group $R\bar{3}$), and over 150 compounds have been reported [8] in which *A* is Sr, Ba, Pd and lanthanides and *M*, *M*' are +2, +3, or +4 metal cations. The *M* and *M*' ions are octahedrally coordinated by oxygen ions, and the MO_6 and $M'O_6$ octahedra are connected by BO_3 triangles. They form a chain-like structure along the *c* axis. From the aspect of magnetochemistry, this structural feature is very attractive because this chain may be regarded as a one-dimensional magnetic chain (*M*–*M*'–*M*–*M*' …) which often shows characteristic magnetic behaviors such as the spin-Peierls transitions [9], Haldane systems [10], and

frustrated spin systems between magnetic chains [11, 12]. In spite of such a structural feature and the existence of many variants in this $A_6MM'(BO_3)_6$ family, their magnetic properties have not been well known for a long time.

In order to characterize magnetic properties of $A_6MM'(BO_3)_6$ compounds, we synthesized a series of iron borates containing lanthanides $Sr_6LnFe(BO_3)_6$. In them, only two compounds (*Ln* = Gd, Ho) have been synthesized up to now [8]. The $Sr_6LnFe(BO_3)_6$ contain two kinds of magnetic ions, Ln^{3+} and Fe^{3+}, and this combination is expected to have the strongest magnetic interaction among the obtainable $A_6MM'(BO_3)_6$ compounds due to that there exist the Fe^{3+} ion having the largest possible spin and the d-f magnetic interaction between Fe^{3+} and Ln^{3+} ions. The compounds for *M* = *M*' = transition metals having the stronger d-d magnetic interaction cannot be obtained because of their smaller ionic radii; the Sc^{3+} (0.745 Å) ion is a lower limit to maintain this crystal structure as reported by Schaffers *et al*. [8].

In this paper, we will report synthesis, crystal structure and magnetic properties for $Sr_6LnFe(BO_3)_6$ (*Ln* = La, Pr, Nd, Sm–Lu) through measurements of their powder X-ray diffraction, magnetic susceptibility and specific heat.

Experimental

Synsthesis of samples

Polycrystalline samples of $Sr_6LnFe(BO_3)_6$ (*Ln* = La, Pr, Nd, Sm–Lu) were synthesized by the standard solid-state reaction. As starting materials, $SrCO_3$, Ln_2O_3, Pr_6O_{11}, Fe_2O_3, H_3BO_3 were used. These starting materials were weighed out in a stoichiometric ratio. For H_3BO_3, ~4 % excess of amounts were added to compensate for the volatilization loss. These starting materials were well mixed in an agate mortar. The mixtures were pressed into pellets and placed on alumina boat, and then they were heated in air at 1273 K for 12 h.

Powder x-ray diffraction measurements

Powder X-ray diffraction (XRD) measurements were performed at room temperature using a Rigaku MultiFlex diffractometer with a Cu-*K*α X-ray radiation source equipped with a curved graphite monochromator. The data were collected by step-scanning in the angle of $10° \leq 2\theta \leq 120°$ at a step size 0.02°. The XRD data were analyzed by the Rietveld method using the RIETAN-FP [13] and the crystal structure was drawn by using the VESTA [14] program.

Magnetic measurements

The temperature dependence of the magnetic susceptibilities was measured with a SQUID magnetometer (Quantum Design, MPMS-5S). The measurements were performed under both zero-field-cooled (ZFC) and field-cooled (FC) conditions over the temperature range 1.8–300 K in an applied magnetic field of 0.1 T.

Specific Heat measurements

The specific heat measurements were performed using a relaxation technique with a commercial physical property measurement system (Quantum Design, PPMS) in the temperature range 1.8–300 K. The pelletized sample was mounted on a thin alumina plate with Apiezon N-grease for better thermal contact.

Results and discussion

Crystal Structure

Polycrystalline samples of $Sr_6LnFe(BO_3)_6$ (*Ln* = La, Pr, Nd, Sm-Lu) were successfully synthesized by the solid-state reaction. They contain a small amount of $LnBO_3$ as an impurity phase. The XRD patterns are shown in Figure 1. All the XRD profiles were indexed on a hexagonal unit cell with a = 12.185–12.338 Å and c = 9.154–9.241 Å. These XRD profiles were analyzed by the Rietveld method, and as the

starting model of analysis, we used the structural data of $Sr_6YFe(BO_3)_6$ reported by Schaffers *et al*. [8]. In this model, the $Sr_6YFe(BO_3)_6$ crystallizes in the hexagonal structure with space group $R\bar{3}$, and Sr and *Ln* ions occupy different crystallographic sites, 18*f* and 3*a*, respectively. However, the calculated profiles showed a poor fit to the observed ones. To improve the fitting, we analyzed the data by assuming the anti-site disorder between Sr and *Ln* sites. Such a disordered arrangement has been found in the isostructural borates $ASr_4La_3(BO_3)_6$ (*A* = Li, Na) [15]. This disorder strongly affects the intensities at lower angle peaks as shown in inset graphs of Figure 1. The calculated profiles are in good agreement with observed ones as shown in Figure 1 and the refined structural parameters and reliability factors are summarized in Table 1. This result indicates that the title compounds have a disordered arrangement between Sr and *Ln* sites, i.e., the exact chemical formula should be represented as $(Sr_{6-x}Ln_x)(Ln_{1-x}Sr_x)Fe(BO_3)_6$.

The schematic crystal structure of $Sr_6LnFe(BO_3)_6$ is illustrated in Figure 2, and some selected bond lengths are listed in Table 2. In this structure, the $(Ln_{1-x}Sr_x)$ and Fe ions occupy the 3*a* and 3*b* sites, respectively, and form the $(Ln_{1-x}Sr_x)O_6$ and FeO_6 octahedra having six equivalent bond lengths due to the site symmetry ($\bar{3}$). These octahedra are connected by three BO_3 triangles, forming one-dimensional chain

structure along the *c* axis. The 18*f* sites are occupied by both Sr and *Ln* ions, and these ions are 9-coordinated by oxygen ions.

Figure 3 shows the variation of lattice parameters for $Sr_6LnFe(BO_3)_6$ as a function of the ionic radius for 6-coordinated Ln^{3+} ions (R_{Ln}^{3+}). Both lattice parameters increase with R_{Ln}^{3+}, indicating the expansion of cell volume with Ln^{3+} ionic radius. The *x* parameter in $(Sr_{6-x}Ln_x)(Ln_{1-x}Sr_x)Fe(BO_3)_6$ is plotted as a function of R_{Ln}^{3+} in Figure 4, and show a monotonous increasing. This result shows that for larger Ln^{3+} ions the 6-coordinated 3*a* site is mainly occupied by Sr^{2+} ions (ionic radius: 1.18 Å), while this site is occupied by Ln^{3+} ions for the case of smaller Ln^{3+} ions. This tendency is also corresponding to the variation of the bond valence sums [16] for 3*a* sites as plotted in Figure 4. For smaller R_{Ln}^{3+} this value is near 3 which is appropriate to the Ln^{3+} ion, and the value decreases to 2 (appropriate to the Sr^{2+} ion) with increasing R_{Ln}^{3+}.

Magnetic properties of $Sr_6LnFe(BO_3)_6$

The temperature dependences of magnetic susceptibility (χ_M) and inverse magnetic susceptibility (χ_M^{-1}) for $Sr_6LnFe(BO_3)_6$ (*Ln* = La, Lu) are shown in Figures 5. Both compounds show a paramagnetic behavior in the whole experimental temperature range (1.8–300 K). No magnetic cooperative phenomena have been observed down to 1.8 K. There is no divergence between ZFC and FC magnetic susceptibility. The magnetic

susceptibility data above 50 K were fitted by the Curie-Weiss law:

$$\chi_{\mathrm{M}} = C/(T-\theta) + \chi_{\mathrm{TIP}} \qquad (1)$$

where the parameters C, θ, χ_{TIP} represent the Curie constant, Weiss constant, temperature-independent magnetic susceptibility, respectively. The effective magnetic moment (μ_{eff}) calculated from $C = N_{\mathrm{A}}\,\mu_{\mathrm{eff}}^2/3k_{\mathrm{B}}$ and Weiss constants are listed in Table 3. The effective magnetic moments are close to the theoretical value 5.92 μ_{B}/Fe for Fe^{3+} ion ($3d^5$, S = 5/2), which indicates that the Fe ions in $Sr_6LnFe(BO_3)_6$ (*Ln* = La, Lu) are in the trivalent state. The small negative Weiss constants (θ) mean that the weak antiferromagnetic interaction exists between Fe^{3+} ions.

The temperature dependences of inverse magnetic susceptibility (χ_{M}^{-1}) for $Sr_6LnFe(BO_3)_6$ (*Ln* = Pr, Nd, Sm–Yb) are shown in Figure 6. These compounds show a paramagnetic behavior in the whole experimental temperature range (1.8–300 K). By applying the Curie-Weiss to the inverse magnetic susceptibility vs. temperature curves, the effective magnetic moments and Weiss constants are obtained. They are listed in Table 3. In these compounds, paramagnetic Fe^{3+} and Ln^{3+} ions are contained. The effective magnetic moments are close to the theoretical values calculated by $\sqrt{\mu_{\mathrm{Fe}^{3+}}^2 + \mu_{Ln^{3+}}^2}$. These results indicate that the Fe ions in $Sr_6LnFe(BO_3)_6$ (*Ln* = Pr, Nd, Sm–Yb) are in the trivalent state. The negative Weiss constants (θ) mean that the

antiferromagnetic interaction is also dominant in these compounds.

In order to clarify the possibility of magnetic ordering at low temperatures, specific heat measurements were carried out for $Sr_6LnFe(BO_3)_6$ (*Ln* = La, Lu). The temperature dependences of the specific heat (C_p) are shown in Figure 7. Below 3 K, the specific heat turns to increase with decreasing temperature. This result implies the onset of long-range magnetic ordering below this temperature, and it may be antiferromagnetic because of the negative Weiss temperature. However, the absolute values of θ are quite small and a clear magnetic transition point was not observed down to 1.8 K. For *Ln* = diamagnetic lanthanide ions (La^{3+} and Lu^{3+}), the nearest interatomic distance between magnetic ions (Fe^{3+}) is 7.7–7.8 Å. Therefore, the magnetic interaction between them should be so weak that the magnetic transition cannot be observed in the experimental temperature range.

On the other hand, for compounds containing magnetic Ln^{3+} ions there exists an additional magnetic interaction between Fe^{3+} and Ln^{3+} ions with an interatomic distance of 4.58–4.61 Å (= *c*/2). From the structural aspect, the existence of this interaction may bring about the low-dimensional magnetic behavior due to the Fe^{3+}–Ln^{3+}–Fe^{3+}–Ln^{3+}… arrangement along the *c* axis. However, the magnetic susceptibility shows not a low-dimensional behavior, but a Curie-Weiss one. This result indicates that the

magnetic interaction between Fe^{3+} and Ln^{3+} ions is very weak because of its long superexchange pathway (Fe–O–O–*Ln* or Fe–O–B–O–*Ln*) and magnetic dilution by Sr^{2+} ion at the Ln^{3+} (3*a*) site. At very low temperatures, the magnetic Ln^{3+} ion may affect the magnetic behavior. The increasing of C_p in the $Sr_6DyFe(BO_3)_6$ is observed at ~5 K (Figure 7), which is somewhat higher than 3 K in *Ln* = La and Lu compounds. This increasing may be due to that the Fe^{3+}–Dy^{3+} magnetic interaction heightens the magnetic transition temperature of $Sr_6LnFe(BO_3)_6$.

Conclusions

The iron borates containing lanthanides $Sr_6LnFe(BO_3)_6$ (*Ln* = La, Pr, Nd, Sm–Lu) were synthesized, and their crystal structure and magnetic properties were investigated. They crystallize in a hexagonal structure with space group $R\bar{3}$, and have a chain structure consisting of FeO_6 and (Ln, Sr)O_6 octahedra connected by BO_3 triangles. They have a disordered arrangement between Sr and *Ln* sites, and the exact chemical formula should be represented as $(Sr_{6-x}Ln_x)(Ln_{1-x}Sr_x)Fe(BO_3)_6$. The 3*a* site is mainly occupied by Sr^{2+} ions for larger Ln^{3+} ions, while this site is occupied by Ln^{3+} ions for smaller Ln^{3+} ions. From the magnetic susceptibility measurements, all compounds show a

paramagnetic behavior. At very low temperatures (~3 K), an onset of antiferromagnetic transition is observed in the specific heat measurements.

References

[1] D. Jaque, J. Capmany, Z.D. Luo, and S.J. Garcia, *J. Phys.: Condens. Matter*, **9**, 9715–9729 (1997).

[2] M. N. Popova, T. N. Stanislavchuk, B. Z. Malkin, and L. N. Bezmaternykh, *Phys. Rev. Lett.*, **102**, 187403 (2009).

[3] Y. Hinatsu, Y. Doi, K. Ito, M. Wakeshima, and A. Alemi, *J. Solid State Chem.*, **172**, 438–445 (2003).

[4] A.K. Zvezdin, S.S. Krotov, A.M. Kadomtseva, G.P. Vorob'ev, Y.F. Popov, A.P. Pyatokov, L.N. Bezmaternykh, and E.A. Popova, 2005 *JETP Lett.*, **81**, 272–276 (2005).

[5] Y. Doi, T. Satou, and Y. Hinatsu, *J. Solid State Chem.*, **206**, 151–157 (2013).

[6] P.D. Thompson and D.A. Keszler, *Chem. Mater.*, **1**, 292–294 (1989).

[7] K.I. Schaffers, T. Alekel III, P.D. Thompson, J.R. Cox, and D.A. Keszler, *J. Am Chem. Soc.*, **112**, 7068–7069 (1990).

[8] K.I. Schaffers, P.D. Thompson, T. Alekel III, J.R. Cox, and D.A. Keszler, *Chem. Mater.*, **6**, 2014–2022 (1994).

[9] M. Hase, I. Terasaki, and K. Uchinokura, *Phys. Rev. Lett.*, **70**, 3651–3654 (1993).

[10] J. Darriet and L.P. Regnault, *Solid State Commun.*, **86**, 409–412 (1993).

[11] M. Mekata and K. Adachi, *J. Phys. Soc. Jpn.*, **44**, 806–812 (1978).

[12] Y. Doi, R. Suzuki, Y. Hinatsu, K. Kodama, N. Igawa, *Inorg. Chem.*, **54**, 10725–10731 (2015).

[13] F. Izumi and K. Momma, *Solid State Phenom.*, **130**, 15–20 (2007).

[14] K. Momma and F. Izumi, *J. Appl. Crystallogr.*, **44**, 1272–1276 (2011).

[15] Q.D. Zeng and R.K. Li, *Solid State Science.*, **29**, 75–78 (2014).

[16] I.D. Brown and D. Altermatt, *Acta Crystallogr. B*, **41**, 244–247 (1985).

Figure cations

Fig. 1 The powder X-ray diffraction profiles for (a) $Sr_6LaFe(BO_3)_6$ and (b) $Sr_6LuFe(BO_3)_6$. The vertical markers show positions calculated from Bragg reflections. The bottom trace is a plot of the difference between the calculated and observed intensities. Insets show the calculation profiles with the different cation occupation at the 3*a* site.

Fig. 2 Schematic crystal structure of $Sr_6LnFe(BO_3)_6$. The lower figure is the structure viewed from the *c*-axis. The *Ln* and Sr ions are located on two kinds of crystallographic sites in a disordered manner: 3*a* (the center of blue octahedra) and 18*f* (orange circles).

Fig. 3 The variation of lattice parameters for $Sr_6LnFe(BO_3)_6$ with 6-coordinated Ln^{3+} ionic radius.

Fig. 4 The *x* parameter in $(Sr_{6-x}Ln_x)(Ln_{1-x}Sr_x)Fe(BO_3)_6$ and the bond valence sums (BVS) for the 3*a* site as a function of 6-coordinated Ln^{3+} ironic radius.

Fig. 5 The temperature dependence of magnetic susceptibility (χ_M) for $Sr_6LnFe(BO_3)_6$ (*Ln* = La, Lu). The inset shows the inverse magnetic susceptibility (χ_M^{-1}), and solid line is the Curie-Weiss fitting in the temperature range 50–300 K.

Fig. 6 The temperature dependence of inverse magnetic susceptibility (χ_M^{-1}) for $Sr_6LnFe(BO_3)_6$ (*Ln* = Pr, Nd, Sm–Yb). The solid line represents the Curie-Weiss fitting in the temperature range 50–300 K.

Fig. 7 The temperature dependence of specific heat divided by temperature (C_p/T) for $Sr_6LnFe(BO_3)_6$ (*Ln* = La, Dy, Lu).

Figures and Tables

Figure 1

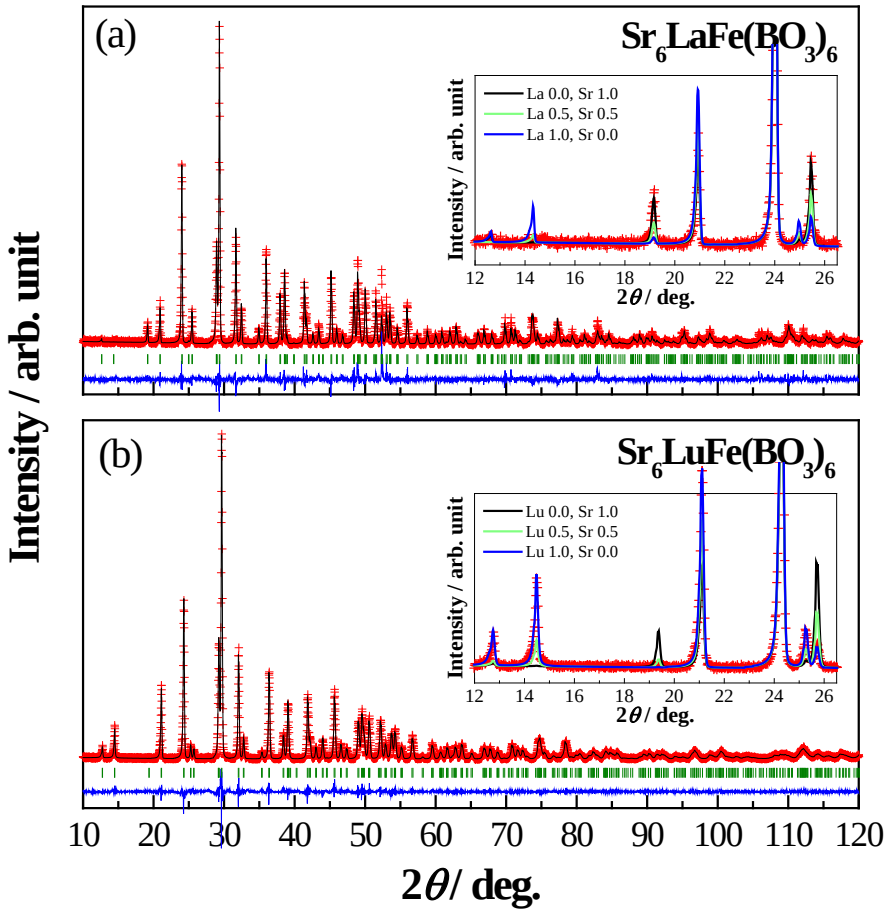

Figure 2

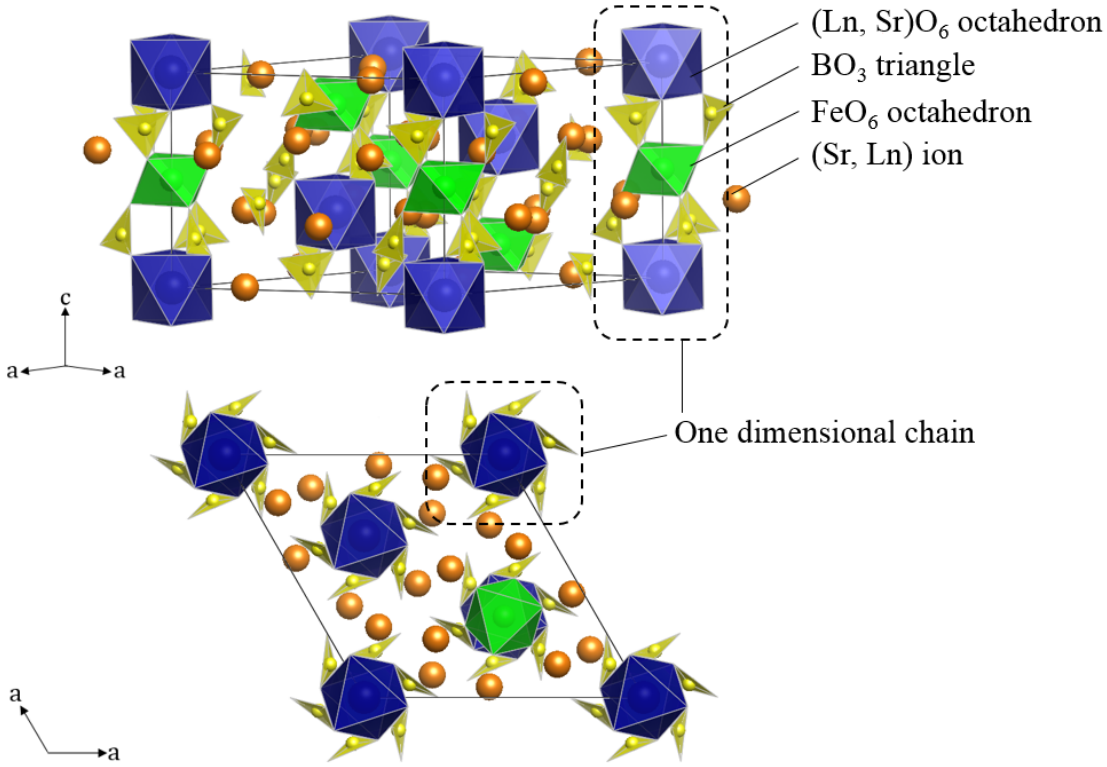
(Ln, Sr)O6 octahedron
BO3 triangle
FeO6 octahedron
(Sr, Ln) ion
One dimensional chain
c
a
a
a
a

Figure 3

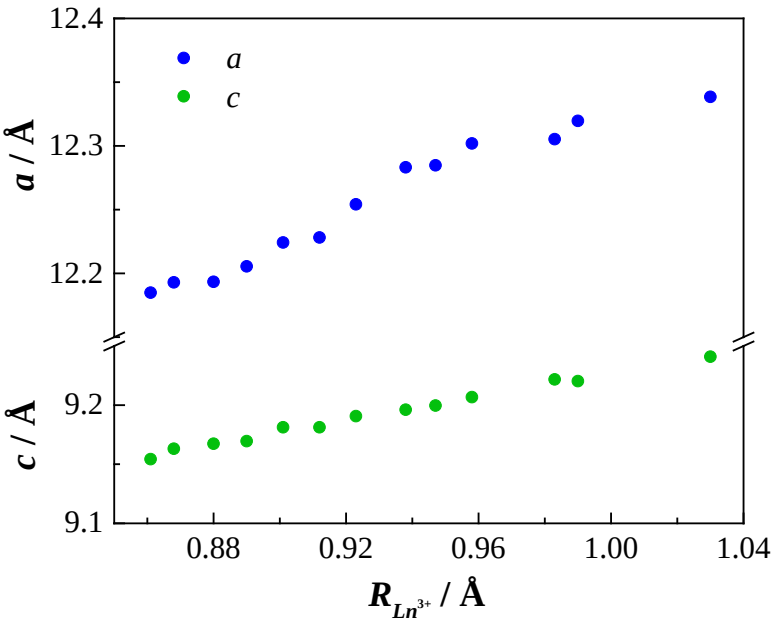

Figure 4

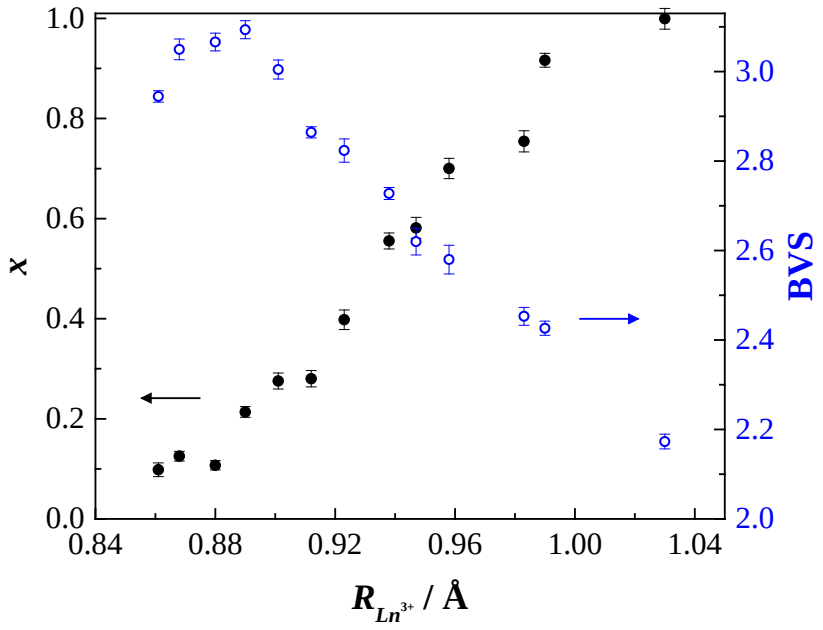
1.0
0.8
0.6
0.4
0.2
0.0
x
3.0
2.8
2.6
2.4
2.2
2.0
BVS
0.84
0.88
0.92
0.96
1.00
1.04
R_Ln3+ / Å

Figure 5

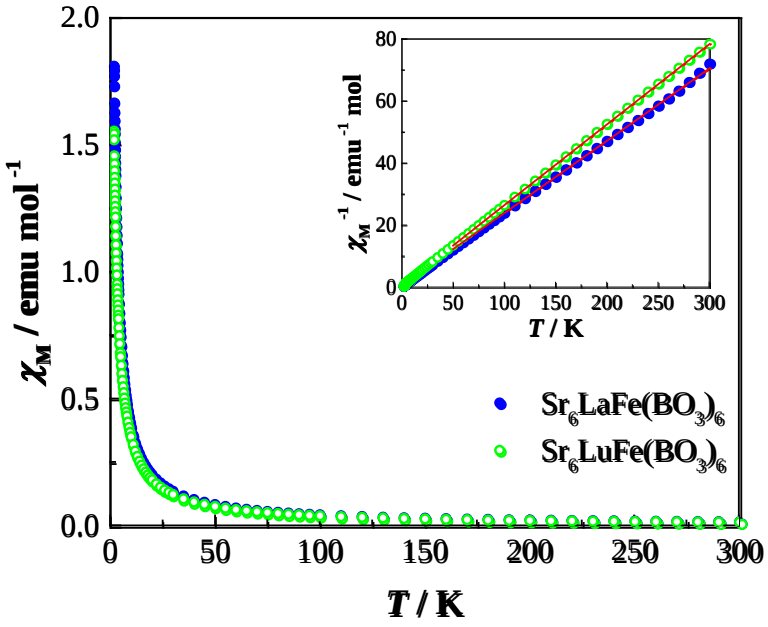
2.0
1.5
1.0
0.5
0.0
0
50
100
150
200
250
300
χM / emu mol-1
T / K
80
60
40
20
0
χM -1 / emu-1 mol
Sr6LaFe(BO3)6
Sr6LuFe(BO3)6

Figure 6

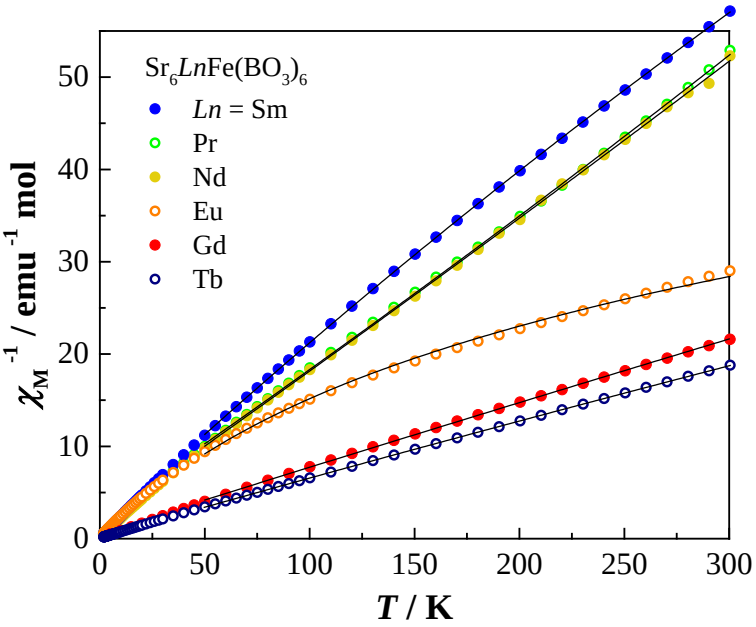
Sr6LnFe(BO3)6
Ln = Sm
Pr
Nd
Eu
Gd
Tb
χM-1 / emu-1 mol
T / K
0
10
20
30
40
50
0
50
100
150
200
250
300

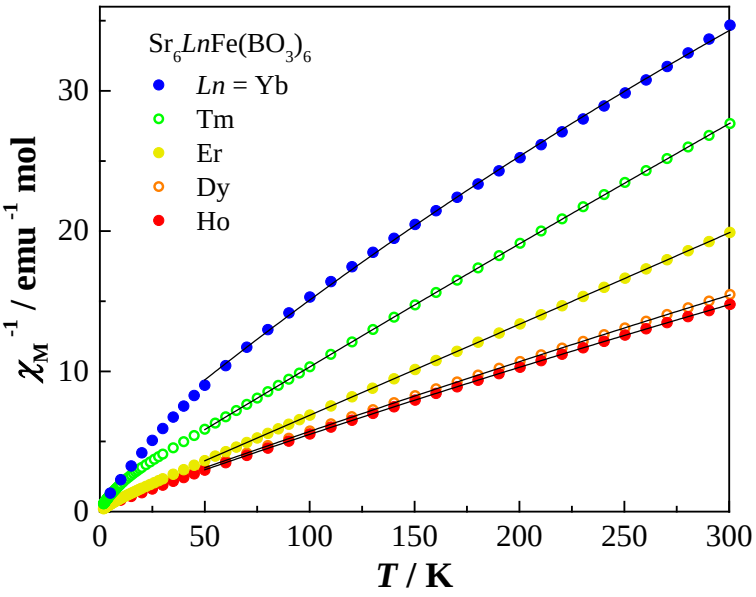
Sr6LnFe(BO3)6
Ln = Yb
Tm
Er
Dy
Ho
χM-1 / emu-1 mol
T / K
0
10
20
30
0
50
100
150
200
250
300

Figure 7

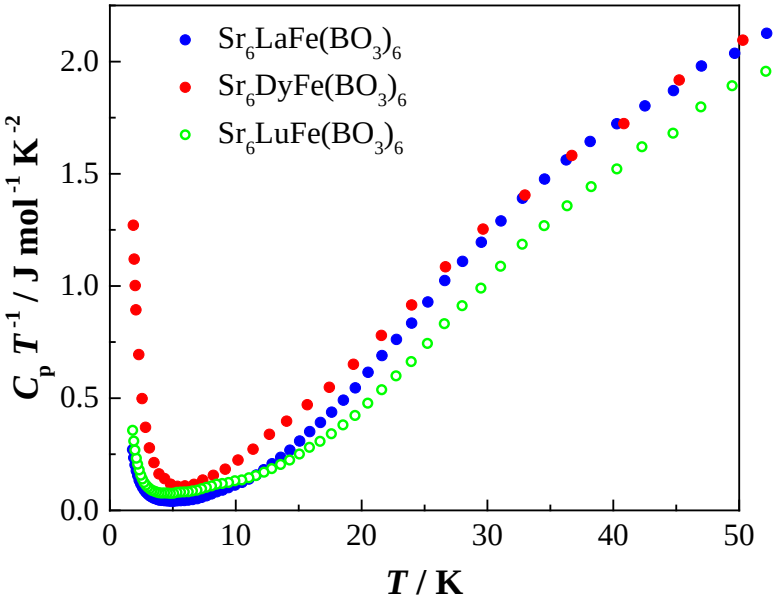
Sr6LaFe(BO3)6
Sr6DyFe(BO3)6
Sr6LuFe(BO3)6
Cp T-1 / J mol-1 K-2
T / K
0.0
0.5
1.0
1.5
2.0
0
10
20
30
40
50

Table 1 Structural parameters for $Sr_6LnFe(BO_3)_6$ (*Ln* = La, Lu) determined by XRD data.

$Sr_6LaFe(BO_3)_6$

Atom	Site	*g*	*x*	*y*	*z*	*B* / Å^2
Space group $R\bar{3}$; *a* =12.3384(7) Å, *c* =9.2409(4) Å, R_{wp} = 17.25 %, R_p = 13.06 %, R_e = 11.81 %, R_B = 5.99 %, R_F = 3.54 %.						
La1	3*a*	0.001(17) = *x*	0	0	0	0.3(1)
Sr1	3*a*	1 – *x*	0	0	0	0.3
Sr2	18*f*	5/6 + *x*/6	0.4707(2)	0.0430(2)	0.6937(2)	0.3
La2	18*f*	1/6 – *x*/6	0.4707	0.0430	0.6937	0.3
Fe	3*b*	1	0	0	1/2	0.2(1)
B	18*f*	1	0.1935(29)	0.0559(35)	0.7563(29)	0.6
O1	18*f*	1	0.2656(16)	0.0005(11)	0.8095(15)	1.0(2)
O2	18*f*	1	0.1600(13)	0.0483(15)	0.6122(15)	1.0
O3	18*f*	1	0.1774(15)	0.1411(15)	0.8296(18)	1.0

$Sr_6LuFe(BO_3)_6$

Atom	Site	*g*	*x*	*y*	*z*	*B* / Å2
Space group $R\bar{3}$; *a* = 12.1849(6) Å, *c* = 9.1542(3) Å, R_{wp} = 13.41 %, R_p = 9.87 %, R_e = 9.53 %, R_B = 3.34 %, R_F = 2.10 %.						
Lu1	3*a*	0.902(11) = *x*	0	0	0	0.4(1)
Sr1	3*a*	1 – *x*	0	0	0	0.4
Sr2	18*f*	5/6 + *x*/6	0.4703(2)	0.0420(1)	0.6947(2)	0.4
Lu2	18*f*	1/6 – *x*/6	0.4703	0.0420	0.6947	0.4
Fe	3*b*	1	0	0	1/2	0.3(1)
B	18*f*	1	0.1933(18)	0.0616(22)	0.7670(20)	0.6
O1	18*f*	1	0.2670(10)	0.0122(8)	0.8112(11)	0.9(2)
O2	18*f*	1	0.1552(10)	0.0440(11)	0.6101(10)	0.9
O3	18*f*	1	0.1578(11)	0.1246(10)	0.8490(13)	0.9

Table 2 Bond lengths (Å) and bond valence sums (BVS) for octahedral sites (3*a* and 3*b*) in $Sr_6LnFe(BO_3)_6$.

Ln	(*Ln*, Sr)–O3×6	BVS (*Ln*, Sr)	Fe–O2×6	BVS (Fe)
La	2.55(1)	2.17	2.04(1)	2.83
Pr	2.47(1)	2.43	2.05(1)	2.70
Nd	2.45(1)	2.45	2.02(1)	2.93
Sm	2.40(2)	2.58	2.03(1)	2.90
Eu	2.38(2)	2.62	2.01(1)	3.02
Gd	2.36(1)	2.73	2.03(1)	2.90
Tb	2.33(2)	2.82	2.03(1)	2.85
Dy	2.31(1)	2.86	1.99(1)	3.24
Ho	2.28(1)	3.00	1.98(1)	3.30
Er	2.25(1)	3.09	1.97(1)	3.36
Tm	2.25(1)	3.07	1.97(1)	3.40
Yb	2.24(1)	3.05	1.96(1)	3.44
Lu	2.23(1)	2.94	1.97(1)	3.43

Note. The BVS values were calculated by $\sum_i \exp((l_0 - l_i)/\mathrm{B})$ where l_i is bond length, parameters l_0 and B are used in "bvparm2013.cif" by IUCr.

Table 3 The effective magnetic moments (μ_{eff}) and Weiss constants (θ) for $Sr_6LnFe(BO_3)_6$.

	La	Pr	Nd	Sm	Eu	Gd	Tb
μ_{eff} / μ_B	5.88(5)	7.19(5)	7.09(6)	6.12(1)	5.99(3)	10.54(4)	11.11(2)
μ_{cal} / μ_B[a]	5.92	6.92	6.94	5.98	5.92	9.90	11.38
θ / K	–2.8(7)	–15.5(11)	–12.6(10)	–4.3(3)	–1.5(2)	–8.5(8)	–3.0(2)

	Dy	Ho	Er	Tm	Yb	Lu
μ_{eff} / μ_B	12.17(3)	12.22(2)	11.14(1)	9.36(1)	7.23(10)	5.53(1)
μ_{cal} / μ_B[a]	12.17	12.12	11.27	9.59	7.46	5.92
θ / K	–8.8(5)	–6.9(3)	–6.2(1)	–14.6(2)	–18.0(20)	–1.1(2)

[a] Calculated effective magnetic moment from $\sqrt{\mu_{Fe^{3+}}^2+\mu_{Ln^{3+}}^2}$, where μ_{Fe}^{3+} = 5.92 μ_B.